Pergamon

0956-7151(95)00086-0

Acta metall. mater. Vol. 43, No. 10, pp. 3669–3678, 1995
Elsevier Science Ltd

0956-7151/95 $9.50 + 0.00

A NEW MODEL FOR THE PEAK OF ACTIVATION AREA OF α TITANIUM

S. FARENC, D. CAILLARD and A. COURET†
CEMES-LOE/CNRS 29, Rue J. Marvig, BP 4347, 31055 Toulouse Cedex, France

(Received 5 August 1994; in revised form 3 February 1995)

Abstract—For prismatic slip in α titanium, the temperature dependence of the activation area peaks at around 350 K in specimens of moderate purity. TEM *in situ* deformation experiments have been performed between 150 and 473 K in order to determine the origin of this peak. In the entire temperature range, rectilinear screw dislocations are found to move by jumps between locking positions. The jump length decreases as the temperature is increased. This last experimental result is at the origin of the present model. This jump length variation leads indeed to several transitions between the microscopic mechanisms controlling the dislocation propagation. For each mechanism, the activation area is calculated as a function of stress. A global evolution of the activation area is obtained and compared with the data reported in the literature.

Résumé—Dans les plans prismatiques du titane α, l'aire d'activation présente un pic prononcé autour de 350 K pour des titanes de pureté moyenne. Des expériences de déformation in situ ont été réalisées entre 150 et 473 K pour rechercher l'origine de ce pic. Dans tout le domaine de température, la déformation est contrôlée par des dislocations vis rectilignes qui glissent par une succession de sauts entre positions de blocage. A partir de ces essais, nous mesurons que la longueur de saut diminue lorsque la température augmente. Ce dernier résultat est à l'origine du modèle présenté dans cet article. Cette variation de la longueur de saut modifie les mécanismes microscopiques contrôlant la propagation des dislocations. Pour chacun de ces mécanismes, l'aire d'activation est calculée en fonction de la contrainte. L'évolution globale de l'aire d'activation ainsi obtenue est comparée aux valeurs macroscopiques.

1. INTRODUCTION

The aim of the present study is to explain the mechanical properties of α titanium when the deformation is accommodated by the glide of *a* dislocations in prismatic planes. In this slip mode, the critical resolved shear stress (CRSS) decreases markedly with temperature and there is a strong hardening effect of the impurity content [1–8]. In titanium of moderate or high impurity ($O^* > 250$ ppm, O^* is the oxygen equivalent concentration), a discontinuity in the temperature dependence of the CRSS associated with a peak in the temperature variation of the activation area has been recorded in a temperature range from 300 to 500 K (Fig. 1 [1, 3–5]). At this impurity level, the magnitude of this peak increases with the level of purity [1, 3, 4]. According to the literature, it seems that this effect is not present in high purity titanium [6, 7]. In such samples, it has been shown that in the low temperature range the activation area is proportional to σ^{-2} [6].

The very high temperature ($T \geqslant 600$ K), in which dynamic strain ageing plays an important role [8], is beyond the scope of the present study.

Post-mortem TEM observations have shown a large density of straight, screw dislocations in prismatic planes [1, 3]. As will be detailed below, *in situ* experiments performed in the low temperature range [9, 10] have shown that plastic deformation is accommodated by the jerky glide of these rectilinear screw dislocations.

The Fleisher type elastic interaction between dislocations and interstitial impurity atoms has been thought to control these mechanical properties [2, 4]. Recent studies and calculations have, however, demonstrated that the glide of dislocations in prismatic planes is controlled by a Peierls type frictional force resulting from a non-planar core structure of the screw dislocations [1, 3, 4, 8–10]; this point will not be discussed here again. Lattice frictional force mechanisms of this type have been reviewed in [11].

When the deformation is controlled by a Peierls type frictional force, dislocations move in a periodical potential with the lattice periodicity. To determine the activation parameters of the controlling mechanisms a key point is to know the critical configuration corresponding to the overcoming of the Peierls valley.

The potential profiles can be of different types depending on the number of minima per period [12]. The sinusoidal potential has only one minimum while the "camel hump" potential has an intermediate

†To whom all correspondence should be addressed.

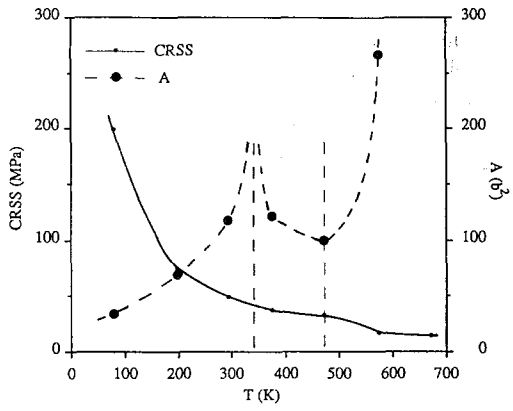

Fig. 1. CRSS (solid rule) and activation area (dashed rule) plotted against temperature (O* = 3270 ppm, from [1, 3])

minimum [Fig. 2(a)]. In both cases, the equilibrium positions of the dislocation are stress dependent. The characteristics of the controlling mechanism (critical shear stress, activation enthalpy and area, and shape of the critical configuration) have been calculated for the sinusoidal and camel hump potentials [13]. Note that in the case of the camel hump potential, a discontinuity in the temperature variation of the activation enthalpy and a peak in the temperature variation of the activation area have been obtained, in agreement with the observations.

According to Friedel [14], when the Peierls force originates from the splitting (or spreading) of the mobile dislocation out of its glide plane, as for instance in the case of HCP metals in prismatic slip and b.c.c. metals, the potential profile shows deeper minima, in which the dislocations split. In what follows, dislocations are assumed to move in such a steep potential which is schematically represented in Fig. 2(b). Dislocations can take two configurations, each corresponding to an energy level which is well defined. The stable, sessile configuration corresponding to a dislocation lying in the Peierls valley is associated with the lower level and the glissile configuration with the higher level. In a first order approximation, the energy of dislocations per unit length is stress independent.

The Friedel's cross-slip mechanism, proposed originally to explain the prismatic glide of h.c.p. metals [15], applies to dislocations lying in such a steep valley. The dislocations are assumed to cross-slip through a thermally activated mechanism from the sessile configuration onto the glissile configuration in the prismatic plane, and to glide freely in this plane. The bowed out critical configuration for this mechanism is shown in Fig. 6(c). In an isotropic medium and within the line tension approximation, the corresponding activation area A_F and height of the arc corresponding to the Friedel critical configuration a_F are given by

$$A_F = \frac{2^{5/2} R^{3/2} \tau^{1/2}}{3\sigma^2 b^2} \tag{1a}$$

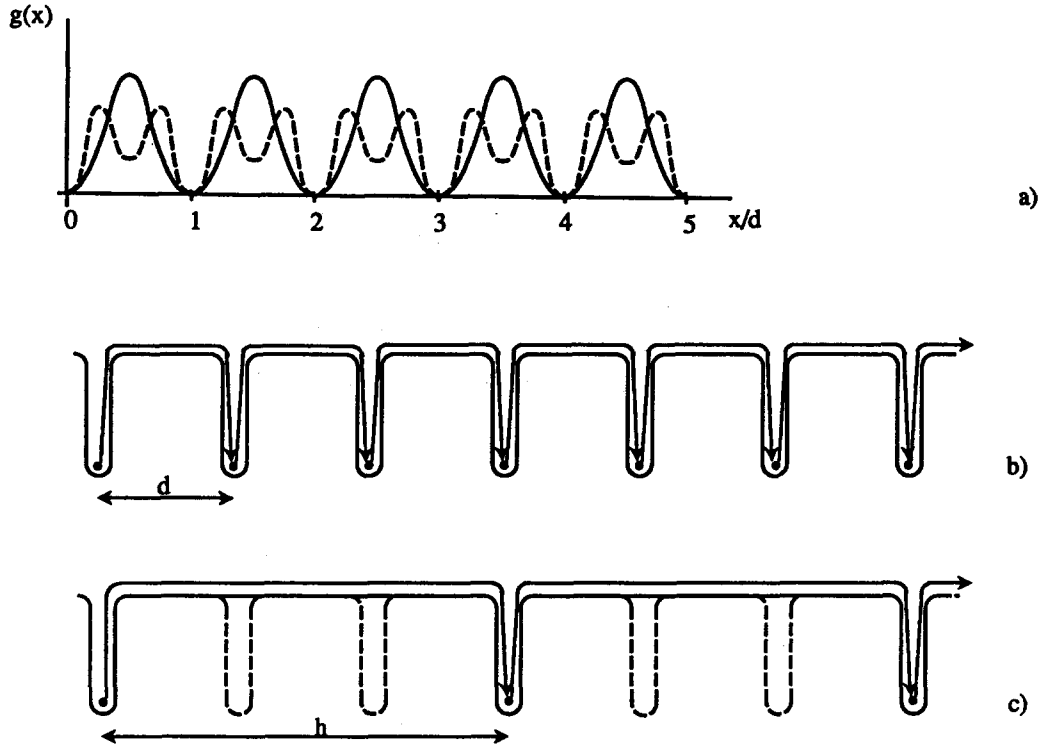

Fig. 2. Functions $g(x)$ giving the profiles of the potentials and schematic description of different types of movements in a steep potential. (a) Sinusoïdal potential (full line) and camel hump potential (dashed line); (b) Peierls mechanism in a steep potential; and (c) locking–unlocking mechanism in a steep potential.

$$a_F = \frac{R}{\sigma b} \tag{1b}$$

where R is the recombination energy namely the difference of energy between the glissile and sessile configurations, τ is the line tension, σ is the shear stress in the glide plane and b is the Burgers vector. It is worth noting that the activation area A_F varies as σ^{-2} in agreement with the experimental data in titanium [6]. This model, however, does not explain the TEM observation of rectilinear screw dislocations in prismatic planes [1, 3] and *in situ* results [9, 10], since it assumes that the dislocations glide freely in the prismatic plane after the first cross-slip event.

On the contrary, the Peierls mechanism explains easily the TEM observations since dislocations are assumed to lie always in the Peierls valleys. Dislocations move between Peierls valleys through the thermally activated nucleation and propagation of kink pairs, the height of which is equal to the distance between two neighbouring Peierls valleys. In such conditions, dislocations move in the potential described schematically in Fig. 2(b). In the case of h.c.p. metals, taking into account the ABAB stacking sequence, the distance d between identical Peierls valleys in the prismatic plane is considered in what follows to be c and not $c/2$ (c is the lattice parameter parallel to the [0001] axis of the hexagonal structure). The theoretical development of such a Peierls mechanism has led to the definition of two stress ranges [16, 17]; the difference between them is illustrated by the shape of the respective critical configurations.

In the high stress range, the critical configuration has the shape of a dislocation bowed in the glide plane and the height of the arc is less than the distance between neighbouring Peierls valleys. This situation is described by the cross-slip model proposed by Friedel [15] discussed above. (Note that in this high stress range, another description has been proposed by Seeger [18] in terms of the line tension approximation. This last approximation leads to a $\log 1/\sigma$ dependence of the activation area.)

In the low stress range, the dislocation reaches the next Peierls valley before the critical configuration of maximum energy is attained [16]. The critical configuration has thus the shape of two or less well separated kinks of opposite signs [Fig. 6(e)]. Various treatments which differ in their initial assumptions on the nature of the kink interaction have been proposed [16–19]. In what follows the kink pair mechanism formulated by Hirth and Lothe [19] will be used. The corresponding activation area $A_{KP}^{(h)}$ is given by

$$A_{KP}^{(h)} = \left(\frac{\mu b h^3}{8\pi\sigma}\right)^{1/2} \tag{2}$$

where μ is the elastic modulus and h is the kink height ($h = d$ for the Peierls mechanism). It is worth noting that the activation area does not depend on the recombination energy and that these relations are only valid in the case of a steep potential. It thus follows that the Peierls mechanism does not explain the σ^{-2} variation of the activation area measured in titanium, except in the high stress range where Friedel's description applies. In this case a discrepancy, however, remains in the order of magnitude of the activation area. Since in this case the height of the critical configuration is smaller than the distance between Peierls valleys, Friedel's description leads indeed to small activation areas of the order of a few tens of b^2 whereas experiments yield activation areas of the order of several hundreds of b^2, at least in titanium.

An alternative mechanism, called locking–unlocking, which was first developed during the study of the prismatic glide of beryllium [20] has been proposed to explain the behaviour of dislocations subjected to such Peierls frictional forces. The potential felt by the dislocation in this model is shown in Fig. 2(c). Dislocations do not fall into all adjacent Peierls valleys but jump over a distance h larger than d between two locking events. This potential is thus similar to a Peierls potential with a longer distance between the valleys. Each jump leads to the formation of a pair of macrokinks the height of which is equal to the jump length. The jump length and the macrokink height are therefore both equal to the distance between two Peierls valleys in which the dislocation has successively cross-slipped. In what follows both distances will be labelled h. The existence of a metastable configuration is at the origin of the difference between Peierls and locking–unlocking mechanisms since it leads to jumps over lengths larger than the distance between Peierls valleys.

Depending on the relative values of h and a_F, two descriptions of this mechanism have been given in the same way as for the Peierls mechanism.

If the arc height a_F of the critical configuration is smaller than the jump length h, the unlocking is described by the Friedel cross-slip mechanism previously explained. The jump length between two locking events is controlled by the probability of locking. The development of the model has shown that the activation parameters of the locking–unlocking mechanism are those of the unlocking mechanism, namely the activation parameters of the Friedel cross-slip mechanism. This mechanism has been proposed to explain the prismatic glide of α titanium in the low temperature range since it explains the σ^{-2} dependence of the activation area and the dynamic microscopic observations [9, 10].

If the jump length is smaller than the arc height, the critical configuration corresponding to the unlocking process is a pair of macrokinks of height equal to the jump length, and the activation area is that given in equation (2) with $h > d$. In this case, locking and unlocking are not independent processes since the jump length which is controlled by the locking probability plays a role in the determination of the activation parameters.

This locking–unlocking mechanism explains the post-mortem TEM observations and the jerky move-

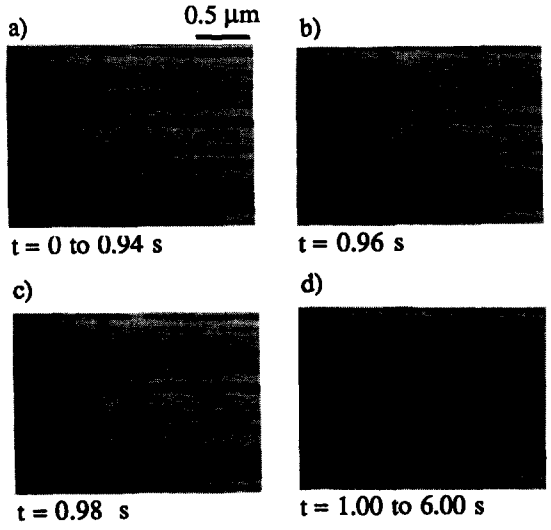

Fig. 3. Jerky movement of a screw dislocation in prismatic plane at 150 K—p_i are locking positions, b is the projection of the Burgers vector.

ments since the dislocations are lying in the Peierls valleys when they are not jumping. It could also explain the σ^{-2} dependence of the activation area measured in the low temperature range, as well as a larger order of magnitude of this parameter, in a better way than the Peierls mechanism since the arc height is larger than the distance between Peierls valleys.

The aim of the present paper is to explain the singularities measured in the temperature dependence of the activation area and CRSS in the framework of the locking–unlocking mechanism. An outline of this explanation has been given in [21]. *In situ* experiments performed above 300 K which are complementary to those described in [9, 10] are also reported in this article. These experiments have been carried out in a titanium ingot provided by S. Naka [1, 3] which has a purity level of O* = 3270 ppm. The experimental procedure can be found in [9, 10, 22].

2. EXPERIMENTAL RESULTS

Figure 3 shows a dislocation with Burgers vector $a = 1/6\langle 11\bar{2}0\rangle$ gliding in a prismatic plane at 150 K. First, it appears that the prismatic slip is due to rectilinear screw segments moving slower than the edge segments, as shown already in [9, 10]. The movement of screw dislocations is jerky. On views (a) and (d), the dislocation under observation is locked at successive positions marked p_i, and the time scale indicates the duration of the sessile positions which appear to be variable. The time scale also indicates that the duration of the sessile position p_2 is less than 1/50 s. The jump times are always much shorter than 1/50 s, since for each jump the starting and final positions are visible on the same video frame because of the remanence of the fluorescent screen [(b) and (c)]. The jump lengths are variable as illustrated below.

Similar dynamic sequences which have been recorded at 200, 300 and 373 K can be seen in [9, 10].

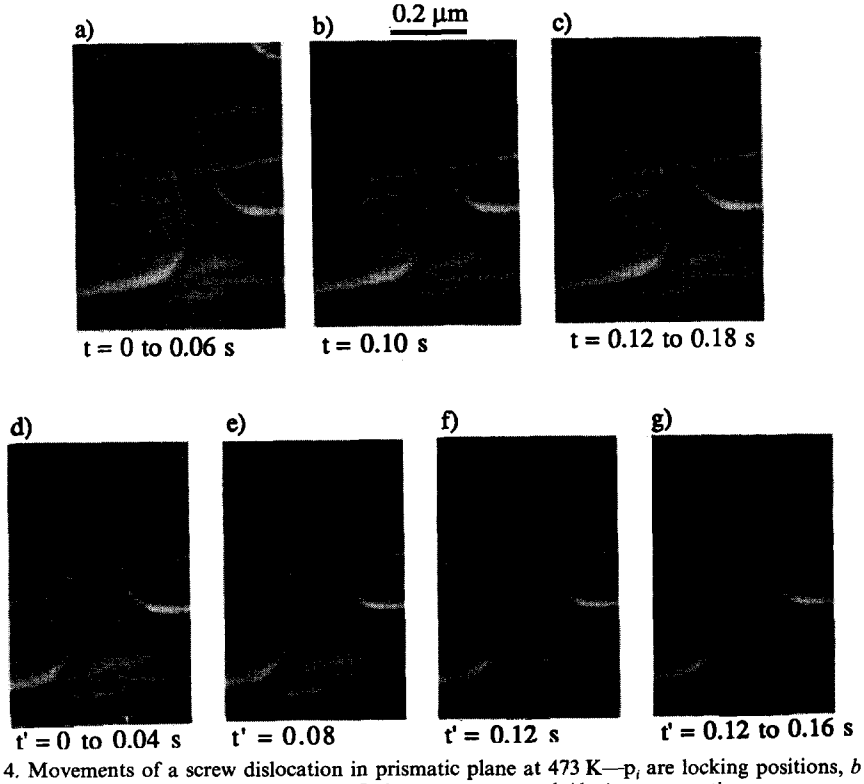

Fig. 4. Movements of a screw dislocation in prismatic plane at 473 K—p_i are locking positions, b is the projection of the Burgers vector. (a–c) Jerky movement; and (d–g) more continuous movement.

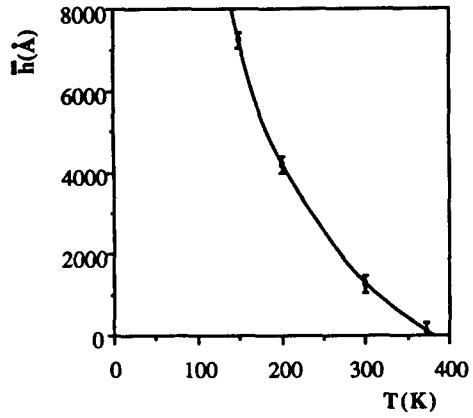

Fig. 5. Plot of the average jump length as a function of temperature.

A similar behaviour has been observed at 473 K [Fig. 4(a)–(c)]. In (a) and (c), a dislocation is locked at positions p_1 and p_2 and in (b), it is jumping between these two positions. Such well identified jumps have been, however, seldom observed at this temperature and most observations were like those shown on pictures (d)–(g) which are four successive pictures of our video record. In (d) and (g) the dislocation is locked at positions p_3 and p_4. In (e) and (f), it is jumping over short distances: the dislocation appears fuzzy and the starting and final positions of the corresponding jumps are not separated because of the jump length being too short.

The jump lengths between locking positions have been measured at different temperatures. At each temperature, such measurements are performed on a short dynamic sequence showing the movement of a set of dislocations of approximately the same length. Under such conditions, it is assumed that all the dislocation considered are moving at yield since the temperature variation of the local stress, which has been deduced from the radii of curvature measurements, reproduces the temperature dependence of the CRSS [9, 10]. To study the influence of temperature on the average jump length, an algebraic average taken from at least 50 measurements has been made at each temperature. Figure 5 shows the temperature dependence of this average jump length $\bar{h}$. The average jump length decreases as the temperature is increased in agreement with a thermally activated locking process. It approaches zero at a temperature ranging between 350 and 400 K.

3. HYPOTHESES OF THE MODEL

The present explanation is based on the idea that the decrease in the average jump length with increasing temperature (Section 2 and Fig. 5) leads to some transitions in the glide mechanism. In what follows, it is assumed that at a given temperature, all the jump

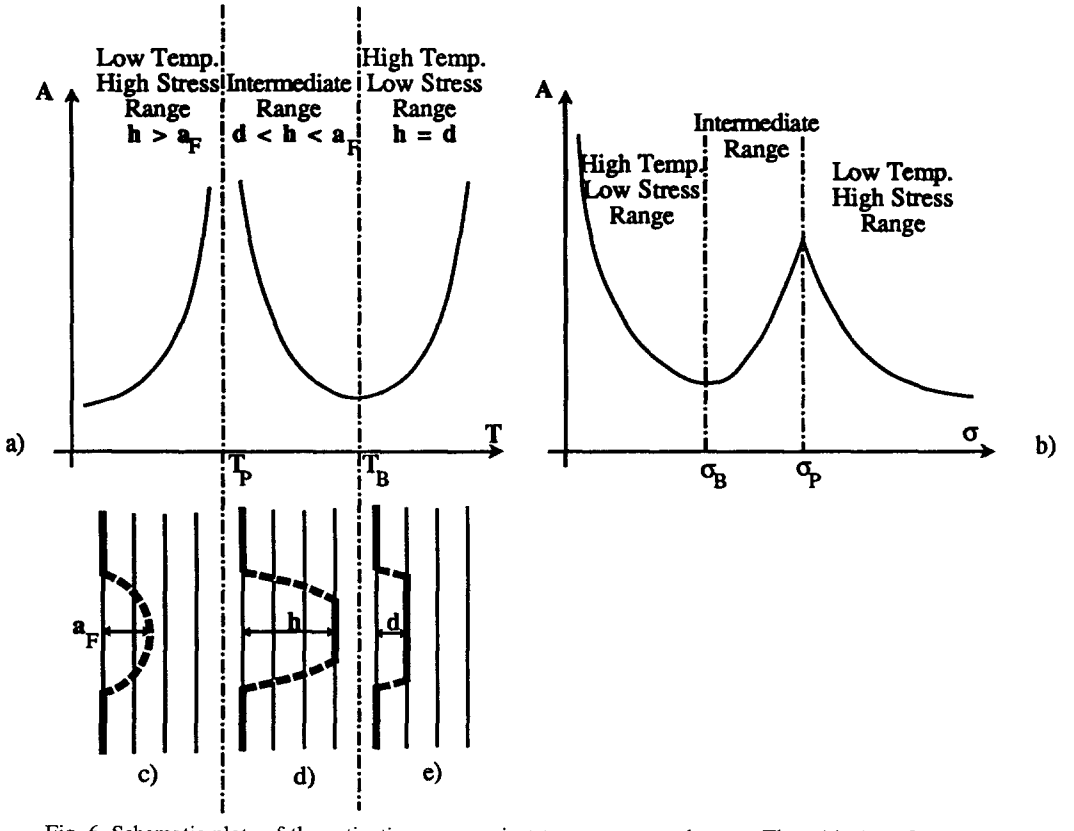

Fig. 6. Schematic plots of the activation area against temperature and stress. The critical configurations corresponding to each range are also shown.

Table 1. Recombination energy calculated from the $\sigma^*(1/\sqrt{A})$ plots and purity of the different titanium ingots (from [1–7])

No.	Ref.	R ($10^{-3}\,\mu b^2$)	Purity
1	[6]	1, 6	O* = 30 ppm, Fe < 10 ppm
2	[6]	2, 1	O* = 50 ppm, Fe = 100 ppm
3	[7]	2, 3	O* = 140 ppm, Fe = 100 ppm
4	[4]	2, 7	O* = 500 ppm
5	[1, 3]	2, 8	O* = 1530 ppm
6	[4]	6, 6	500 ppm < O* < 10,000 ppm
7	[1, 3]	12	O* = 3270 ppm

lengths and thus the kink heights are equal to the average value measured at this temperature.

From the above remark, the following assumptions are made. Figure 6(a) is a schematic description of the activation area vs temperature curve shown in Fig. 1, and Fig. 6(b) shows the same activation area as a function of the corresponding yield stress.

- In the low temperature–high stress range ($T < T_P$ and $\sigma > \sigma_P$), the average jump length $\bar{h}$ is larger than the corresponding arc height a_F. The critical configuration is a dislocation bowed in the glide plane [Fig. 6(c)]. Dislocation movements are controlled by the locking–unlocking mechanism [9, 10] and the activation parameters are those of the Friedel's mechanism.
- At T_P and σ_P, the average jump length is equal to the arc height.
- In the intermediate range ($T_P < T < T_B$ and $\sigma_B < \sigma < \sigma_P$), the average jump length is less than the arc height but larger than d. Accordingly, the critical configuration is a macrokink pair with a height equal to the average jump length [Fig. 6(d)]. The dislocation movement is still controlled by the locking-unlocking mechanism. The activation parameters are, however, those of the kink pair mechanism with $h > d$ as explained in the introduction.
- At T_B and σ_B, the average jump length becomes equal to the distance d between Peierls valleys.
- In the high temperature–low stress range ($T > T_B$ and $\sigma < \sigma_B$), the deformation is controlled by the Peierls mechanism, that is to say the kink pair mechanism with $h = d$. The critical configuration is a kink pair [Fig. 6(e)].

4. STRESS DEPENDENCE OF THE ACTIVATION AREA

In this section, an attempt is made to calculate the stress dependence of the activation area.

4.1. Friedel's mechanism

In the low temperature–high stress range, the activation area is given by relation (1a). Before calculating the activation area as a function of the stress, the line tension τ and the recombination energy R should be evaluated. The line tension τ has been calculated using the relationship given in [19, p. 177]: $\tau = 10^{-1}\mu b^2$ with $\mu = 3.5 \cdot 10^4$ MPa. For titaniums with different purity levels, the recombination energy R has been deduced from the macroscopic data of literature on the basis of relation (1a). The plot of σ^* vs $(1/\sqrt{A})$, where σ^* is the effective stress ($\sigma^* = \text{CRSS} - \sigma_i$ where σ_i is the internal stress, i.e. the CRSS at the athermal temperature) leads to a straight line in agreement with relation (1a), the slope of which gives the recombination energy. The results of this evaluation are given in Table 1. It is worth noting that the recombination energy increases with the impurity content, in agreement with the explanation of the hardening effect by impurities given in [1, 3, 9, 10].

From relations (1a) and (1b), the stress dependences of the activation area $A_F(\sigma)$ and critical arc height $a_F(\sigma)$ can be calculated for different values of R. Calculations have been made for $R = 2.75\ 10^{-3}\,\mu b^2$ because the results will be compared with

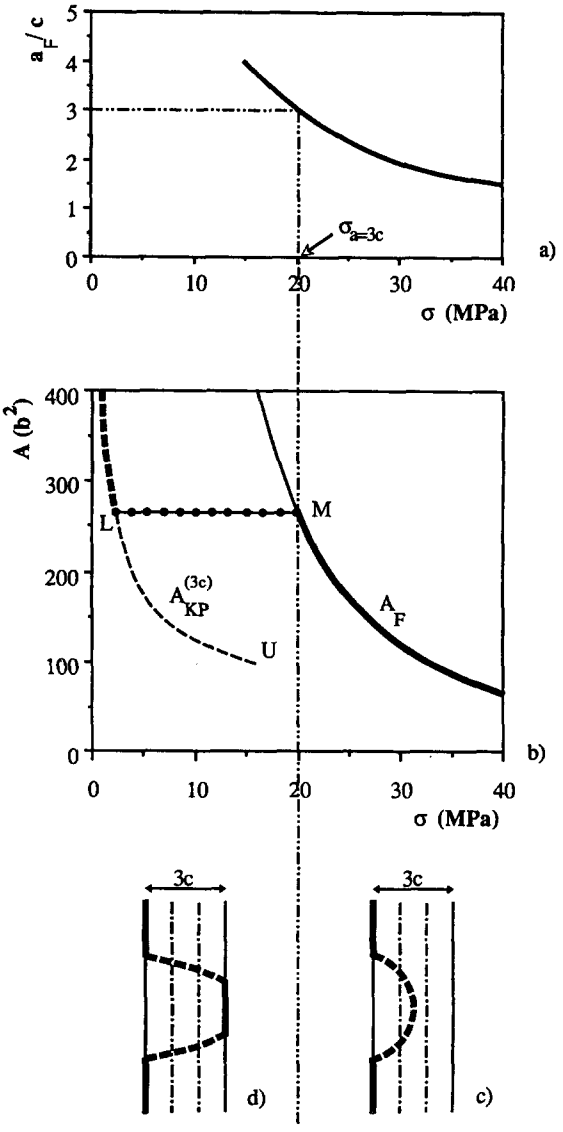

Fig. 7. Arc height (a) and activation area (b) plotted against stress for Peierls valleys separated by 3c. The critical configurations corresponding to the two stress ranges are represented in (c and d).

the macroscopic values obtained in the titanium ingots labelled 4 and 5 in Table 1. They correspond to the curves in Figs 7–9.

4.2. Kink pair mechanism

In the intermediate and high temperature ranges, the deformation is controlled by the kink pair mechanism presented in the Introduction, with a kink height equal to the average jump length. Let us consider kinks of heights c, $2c$, $3c$ and $4c$. Figure 2(b and c) shows the Peierls potential profiles in which the dislocation is moving for $h = c$ and $3c$, respectively.

The development of the kink pair mechanism given by Hirth and Lothe [19] applies if the kink separation corresponding to the critical configuration is larger than the kink width. This leads to the determination of an upper limit of the stress σ_U which is the limit of validity of the Hirth and Lothe treatment

$$\sigma_U = \frac{\mu b}{8\pi h} tg^2 \sqrt{\frac{2R}{\tau}}.$$

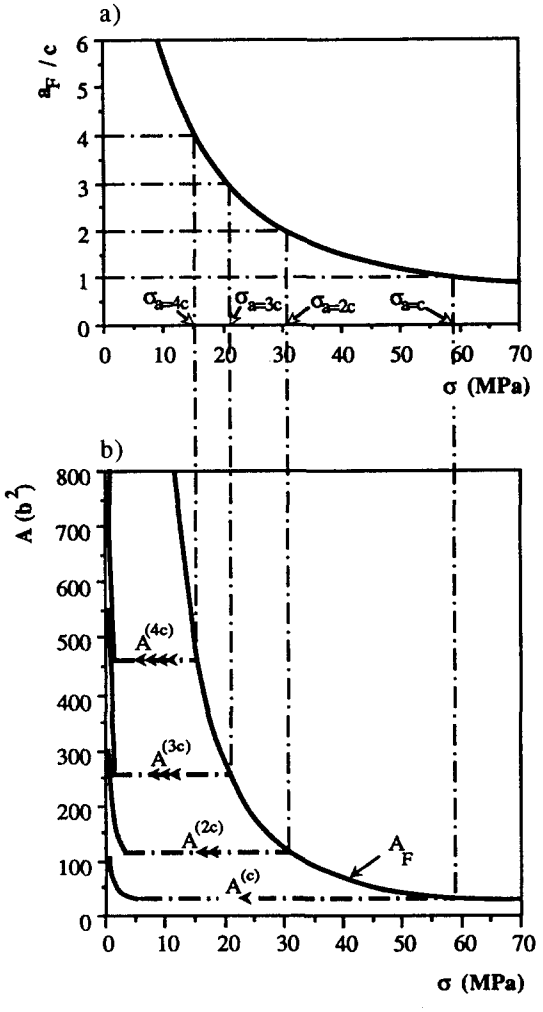

Fig. 8. Arc height (a) and activation area (b) plotted against stress for Peierls valleys separated by c, $2c$, $3c$ and $4c$.

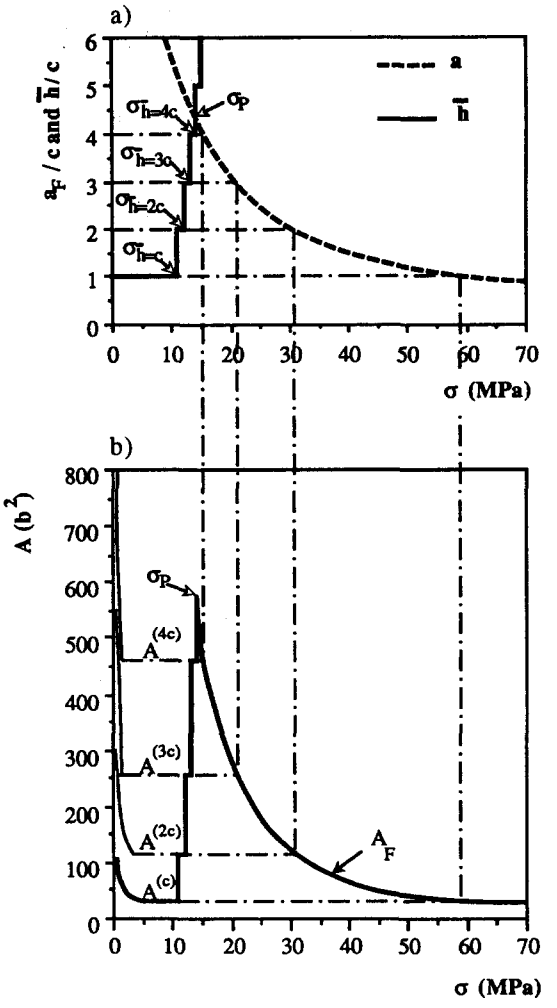

Fig. 9. (a) Arc height (dashed rule) and jump length (solid rule) plotted against stress; and (b) global plot of the activation area against stress.

Estimations of σ_U values for $h = c$, $2c$, $3c$, and $4c$ are given in Table 2 for $R = 2.75\ 10^{-3}\ \mu b^2$. From relation (2), the stress dependence of the activation area $A_{KP}(\sigma)$ have been calculated in the domain of validity. The results are shown in Figs 7–9.

4.3. Stress dependence of the activation area $A^{(h)}(\sigma)$ for a fixed jump length h

Let us assume in this section that the average jump length is constant in the entire temperature range, that is to say the dislocations move between Peierls valleys separated by this length. The kink pair mechanism will be compared to the Friedel mechanism. The corresponding potential profile is that shown on Fig. 2(c), where the jump length has been taken to be $h = 3c$.

Figure 7(a and b) shows in full lines the stress dependences of the critical arc height $a_F(\sigma)$ and activation area $A_F(\sigma)$ for $R = 2.75\ 10^{-3}\ \mu b^2$. In Fig. 7(b) the stress dependence of the activation area for the kink pair mechanism for $h = 3c$, $A_{KP}^{(3c)}(\sigma)$, is also plotted as dashed line. U is the point corresponding

Table 2. Upper limit of validity of the Hirth and Lothe treatment for different values of h

h	σ_U (MPa)
c	47
$2c$	23
$3c$	16
$4c$	11.75

to the limit of validity of the Hirth and Lothe treatment.

$\sigma_{a=3_c}$ is the stress at which $a_F = 3c$ [Fig. 7(a)]. M is the corresponding point on the curve $A_F(\sigma)$ [Fig. 7(b)].

For $\sigma > \sigma_{a=3c}$, since $a_F < 3c$, the dislocation first reaches the Friedel critical configuration [Fig. 7(c)] and subsequently falls in the neighbouring Peierls valley distant of $3c$, thus forming a pair of macrokinks. The corresponding activation area is $A(\sigma) = A_F$, plotted as a heavy full line [Fig. 7(b)].

For $\sigma < \sigma_{a=3c}$. The dislocation falls in the neighbouring Peierls valley distant of $3c$ before reaching the critical configuration. The critical configuration is therefore a macrokink pair with $h = 3c$ [Fig. 7(d)]. L is the point at which $A_{KP}^{(3c)}$ is equal to $A_F(\sigma_{a=3c})$ [Fig. 7(b)]. Note that σ_L is smaller than σ_U, the upper limit of validity of the Hirth and Lothe treatment. For stresses smaller than σ_L, the activation area $A(\sigma)$ is $A(\sigma) = A_{KP}^{(3c)}$, shown as a bold dashed rule. In the stress range between L and M where the kink pair mechanism with a fixed jump length is rate controlling, the activation area is constant and follows a straight horizontal line (dotted line) as shown in the Appendix.

The set of heavy rules (full, dotted and dashed) corresponds therefore to the stress dependence of the activation area of dislocations moving in the Peierls potential profile described on Fig. 2(c). This curve is labelled $A^{(3c)}(\sigma)$ in what follows.

Following the same principle, one can establish a set of $A^{(h)}(\sigma)$ curves. For each one it is assumed that the jump length h is constant in the entire temperature range. In Fig. 8, the curves $A^{(c)}(\sigma)$, $A^{(2c)}(\sigma)$, $A^{(3c)}(\sigma)$ and $A^{(4c)}(\sigma)$, have been plotted. The number of arrows refers to the jump length.

4.4. Global stress dependence of the activation area $A(\sigma)$

The experimental decrease of the average jump length $\bar{h}$ with increasing temperature results in a variation of the apparent periodicity of the Peierls potential. As the stress increases, owing to the corresponding decrease of temperature, the periodicity of the apparent potential increases from c to higher values. In Fig. 9(a), a variation of the jump length $\bar{h}$ describing such a potential variation has been plotted as a full line. A stepped curve has been used because the jump length should be an integer number of c. $\sigma_{\bar{h}=c}$ is the higher stress for which $\bar{h} = c$. $\bar{h} = 2c$ for a stress ranging between $\sigma_{\bar{h}=c}$ and $\sigma_{\bar{h}=2c}$, and so on. The stress $\sigma_{\bar{h}=c}$ has been chosen because it corresponds to the yield stress at 350 K, the temperature at which the average jump length becomes close to the distance between Peierls valleys (Fig. 5). It should, however, be stated that the curve of Fig. 5 has been recorded in the titanium containing O* = 3270 ppm of impurities whereas the present calculations are made for $R = 2.75\,10^{-3}\,\mu b^2$, a value corresponding to a titanium containing a smaller amount of impurities. This point is, however, of minor importance, as it will be discussed in the following section.

In Fig. 9(a and b), the curve $a_F(\sigma)$ and the curves $A_F(\sigma)$, $A^{(c)}(\sigma)$, $A^{(2c)}(\sigma)$, $A^{(3c)}(\sigma)$ and $A^{(4c)}(\sigma)$ have also been plotted.

σ_P is the stress at which $a_F(\sigma)$ intersects $\bar{h}(\sigma)$ [Fig. 9(a)].

For $\sigma > \sigma_P$, since $a_F < \bar{h}$, the critical configuration and the activation area are those of Friedel's mechanism ($A = A_F$).

For $\sigma < \sigma_P$, the average jump length is less than the arc height and the dislocation falls in a Peierls valley before reaching the Friedel critical configuration. The critical configuration is therefore a kink pair, the height of which is the average jump length. At σ_P, since $\bar{h} = 4c$, the A(σ) variation deviates from the $A_F(\sigma)$ curve and drops by following the vertical line to join the curve $A^{(4c)}(\sigma)$. At $\sigma_{\bar{h}=3c}$, which is the upper limit of the stress to have an average jump length of $3c$, it deviates from $A^{(4c)}(\sigma)$ and drops down to $A^{(3c)}(\sigma)$. At $\sigma_{\bar{h}=2c}$, it joins $A^{(2c)}(\sigma)$. At $\sigma_{\bar{h}=c}$, it joins $A^{(c)}(\sigma)$ and follows it till the zero stress.

The heavy full line in Fig. 9(b) which shows the global $A(\sigma)$ curve exhibits a peak. In the following section, it will be compared with the experimental data.

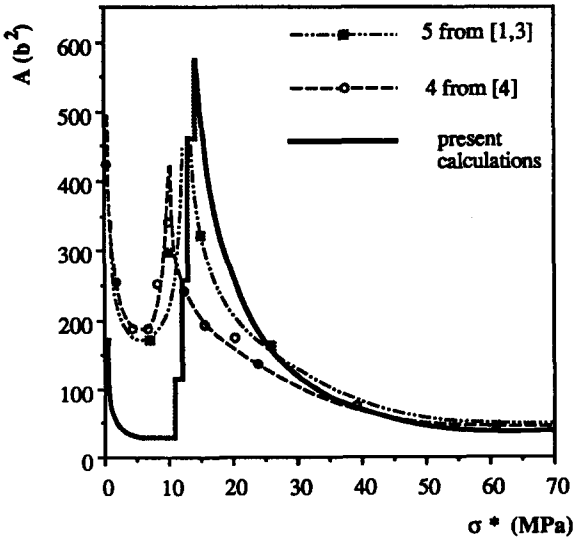

Fig. 10. Comparison between the present calculation and the experimental data from [1, 3, 4]. For the experimental data the effective stress σ^* has been used ($\sigma^* = \text{CRSS} - \sigma_i$ where σ_i is the internal stress, i.e. the CRSS at the athermal temperature).

5. DISCUSSION

In Fig. 10, the stress dependence of the activation area, calculated in the preceding section for $R = 2.75\ 10^{-3}\ \mu b^2$, is compared with that measured in titanium ingots labelled 4 and 5 in Table 1 for which $R = 2.7$ and $2.8\ 10^{-3}\ \mu b^2$, respectively. The present calculations are seen to reproduce the experimental data, especially the peak of activation area.

From the *in situ* experiments performed in the titanium 7, the average jump length has been shown to decrease as the temperature is increased, and to reach the interatomic distance at a temperature between 350 and 400 K. According to the present model, this temperature should be close to the peak temperature. This is in a good agreement with the macroscopic data leading to a peak temperature of 350 K [1, 3]. For that reason, since the peak temperature does not depend too much on the impurity content [1, 3], the curves $\bar{h}(\sigma)$ are thought to increase in all cases above a stress level which corresponds to the CRSS at 350 K. The exact value of the slope of the curve $\bar{h}(\sigma)$ does not have a strong influence since a significant variation of the slope leads just to a small variation of σ_p. For instance, a variation of the slope of a factor 5 will change σ_p from 14 to 20 MPa. This last point will be reinforced by the following remark.

It has been assumed in these calculations that at a given stress all the jump lengths are equal to the average jump length. In practice, as shown experimentally and theoretically in [9, 20], the jump lengths follow an exponential distribution at each temperature. In such conditions, the macroscopic experimental curve is the result of a smoothing of the theoretical ones.

The present model is based on several assumptions: the profile of the potential is steep, the calculations have been made in the frame work of the line tension approximation, the low temperature range is described by the Friedel's mechanism and the Hirth and Lothe formulation of the kink pair mechanism has been used. It should, however, be noted that the peak of activation area is only the result of a decrease of a thermally activated average jump length till a value smaller than the critical arc height. It is thus probable that alternative microscopic description based on the same explanation would yield similar results.

An alternative explanation has been proposed in [13] for the A vs σ curve on the basis of experimental results in b.c.c. metals. This model considers that the dislocations are gliding in a "camel hump" potential (Fig. 2) and that under stress the dislocations are not lying in the minima of the valleys. Till now this model does not, however, explain the σ^{-2} dependence of the activation area and the jerky glide of dislocations which have been observed in titanium.

The explanation proposed in the present paper for the prismatic glide of titanium should also be considered in the case of prismatic glide of magnesium [23] and in the case of b.c.c. metals [24] where similar variations of activation areas have been measured.

6. CONCLUSION

In this work, the peaks in the temperature and stress dependences of the activation in α titanium have been explained by introducing several transitions between the microscopic mechanisms controlling the dislocation glide. Dislocations are assumed to glide in a steep Peierls potential, however, by jumps over variable distances which can range between interatomic distances (classical Peierls mechanism) and large distances (locking–unlocking mechanism). Transitions between different mechanisms are the consequence of a thermally activated decrease of the jump length measured experimentally by means of *in situ* experiments. At low temperatures, since the jump length is larger than the arc height of the Friedel critical configuration, the deformation is controlled by the locking–unlocking mechanism and the activation parameters are those of the Friedel's cross-slip. At high temperatures, since the jump length is less than this critical value, the critical configuration is a macrokink pair and the activation parameters are those of the kink pair mechanism. The height of these kinks is equal to the jump length and varies with temperature.

This model explains in a consistent way two aspects of the deformation which could not be accounted for previously, namely a large density of rectilinear screw dislocations in post-mortem TEM observations and a jerky movement of these dislocations during *in situ* TEM experiments. It also explains the macroscopic σ^{-2} dependence of the activation area measured in the low temperature range.

Acknowledgement—The authors are grateful to Shigehisa Naka for kindly providing the alloy No. 7.

REFERENCES

1. S. Naka, Thèse d'Etat, Université d'Orsay, Paris, France (1983).
2. T. Tanaka and H. Conrad, *Acta metall.* **20,** 1019 (1972).
3. S. Naka, A. Lasalmonie, P. Costa and L. P. Kubin, *Phil. Mag. A* **57,** 717 (1988).
4. A. Akhtar and E. Teghtsoonian, *Metall. Trans. A* **6A,** 2201 (1975).
5. Z. Trojanova, P. Lukac and M. Hamersky, *Acta Univ. Carolin.—Math. Phys.* **32,** 69 (1991).
6. M. P. Biget and G. Saada, *Phil. Mag. A* **59,** 747 (1989).
7. E. D. Levine, *Trans Am. Inst. Min. Engrs* **236,** 1558 (1966).
8. S. Naka, L. P. Kubin and C. Perrier, *Phil. Mag. A* **63,** 1035 (1991).
9. S. Farenc, Thèse d'Université, No. 1131. Toulouse, France (1992).
10. S. Farenc, D. Caillard and A. Couret, *Acta metall.* **41,** 1019 (1993).
11. A. Couret and D. Caillard, *Journal de Physique III* **1,** 885 (1991).
12. P. Guyot and J. E. Dorn, *Can. J. Phys.* **45,** 983 (1967).
13. H. Koizumi, H. O. Kirchner and T. Suzuki, *Acta metall. mater.* **41,** 3483 (1993).

14. J. Friedel, *Phil. Mag.* **46,** 1169 (1955).
15. J. Friedel, in *Internal Stresses and Fatigue in Metals* (edited by G. M. Rassweiler and W. L. Grube), p. 220. Elsevier, Amsterdam (1959).
16. B. Escaig, *Physica status solidi* **28,** 463 (1968).
17. M. S. Duesbery and P. B. Hirsch, in *Dislocations Dynamics* (edited by A. R. Rosenfild, G. T. Hahn, A. L. Bement and R. I. Jaffe), Vol. 57. McGraw–Hill, New York (1967).

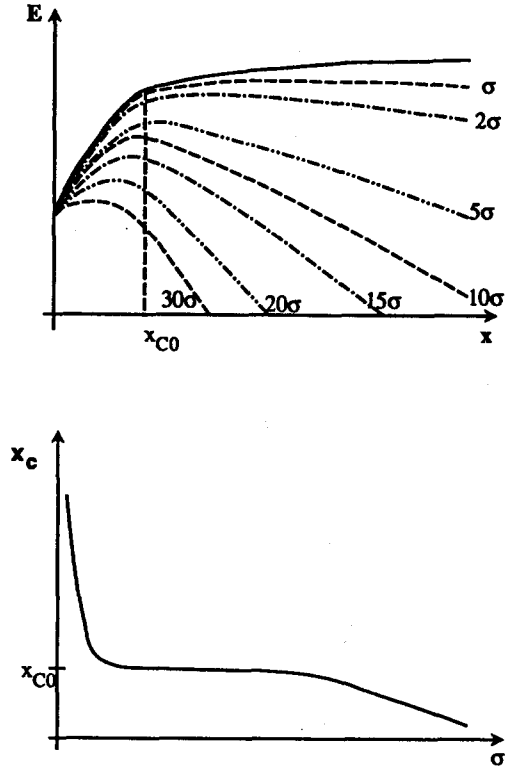

Fig. A1. (a) Energy of a kink pair under zero stress (solid rule) and under different stresses (dashed rule); and (b) variation of x_c vs stress deduced from (a).

18. A. Seeger, *Z. Metallk.* **72,** 369 (1981).
19. J. P. Hirth and J. Lothe, in *Theory of Dislocations.* Wiley–Interscience, New York (1982).
20. A. Couret and D. Caillard, *Phil. Mag. A* **59,** 783 (1989a); *ibid.* **59,** 801 (1989b).
21. S. Farenc, D. Caillard and A. Couret, *Proc. Int. Meet. Aussois (France), Solid State Phenom.* **35–36,** 429 (1994).
22. A. Couret, J. Crestou, S. Farenc, G. Molénat, N. Clément, A. Coujou and D. Caillard *Microsc. Microanal. Microstruct.* **4,** 153 (1993).
23. A. Couret and D. Caillard, *Acta metall.* **33,** 1447 (1985).
24. L. P. Kubin and B. Jouffrey, *Phil. Mag. A* **27,** 1369 (1973).
25. M. S. Duesbery, *Acta metall.* **31,** 1759 (1983).

APPENDIX

It is assumed as in Section 4.3 that the kink pair mechanism with a constant jump length is rate controlling in the whole stress range. The aim of the present Appendix is to discuss the intermediate range lying between points L and M of Fig. 7(b).

In the Figure A1(a), the energy E under zero stress of a dislocation forming a kink pair has been plotted as a function of the kink separation x. Such a variation has been obtained by computer calculations in the case of b.c.c. metals [25]. The change of slope for x_{c0} is related to the existence of the two critical configurations discussed in the text: for $x < x_{c0}$ the kinks are not yet formed and the critical configuration is a bowed out dislocation, whereas for $x > x_{c0}$ the kinks are well formed and the energy increases less quickly as a function of x. The energy of this dislocation under stress can be estimated by including the work done by the applied stress ($w = \sigma bx$). The results are shown in Fig. A1(a), as dashed rules for different relative values of the stress taken in an arbitrary unit. The energy goes through a maximum which gives the activation energy ΔH and the kink separation x_c of the critical configuration which is related to the activation area. Figure A1(b) shows the variation of x_c as a function of stress which has been deduced from Fig. A1(a). Due to the change of slope of $E(x)$, x_c is constant and close to x_{c0} in the intermediate stress range. It follows that the activation area should be almost constant in this stress range in agreement with the assumption made in Section 4.3.